

1 **Revised March 18, 2020**

2 **Conductance mechanisms of rapidly desensitizing cation channelrhodopsins from**
3 **cryptophyte algae**

4 Oleg A. Sineshchekov¹, Elena G. Govorunova¹, Hai Li¹, Yumei Wang¹, Michael Melkonian²,
5 Gane K.-S. Wong^{3,4}, Leonid S. Brown⁵ and John L. Spudich^{1#}

6 ¹Center for Membrane Biology, Department of Biochemistry & Molecular Biology, The
7 University of Texas Health Science Center at Houston McGovern Medical School, Houston,
8 Texas, USA

9 ²Institute of Botany, Cologne Biocenter, University of Cologne, Cologne, Germany

10 ³Departments of Biological Sciences and of Medicine, University of Alberta, Edmonton, Alberta,
11 Canada

12 ⁴Beijing Genomics Institute-Shenzhen, Shenzhen, China

13 ⁵Department of Physics and Biophysics Interdepartmental Group, University of Guelph, Guelph,
14 Ontario, Canada.

15 Running title: Rapidly desensitizing cation channelrhodopsins

16 # Address correspondence to John L. Spudich, john.l.spudich@uth.tmc.edu.

17 Word count Abstract: 334

18 Word count Text: 4,619

19

Rapidly desensitizing cation channelrhodopsins

20 ABSTRACT

21 Channelrhodopsins guide algal phototaxis and are widely used as optogenetic probes for
22 control of membrane potential with light. “Bacteriorhodopsin-like” cation channelrhodopsins
23 (BCCRs) from cryptophytes differ in primary structure from other CCRs, lacking usual residues
24 important for their cation conductance. Instead, BCCR sequences match more closely those of
25 rhodopsin proton pumps, containing residues responsible for critical proton transfer reactions.
26 We report 19 new BCCRs, which, together with the earlier 6 known members of this family,
27 form three branches (subfamilies) of a phylogenetic tree. Here we show that the conductance
28 mechanisms in two subfamilies differ with respect to involvement of the homolog of the proton
29 donor in rhodopsin pumps. Two BCCRs from the genus *Rhodomonas* generate photocurrents
30 that rapidly desensitize under continuous illumination. Using a combination of patch clamp
31 electrophysiology, absorption and Raman spectroscopy, and flash photolysis, we found that the
32 desensitization is due to rapid accumulation of a long-lived nonconducting intermediate of the
33 photocycle with unusually blue-shifted absorption with a maximum at 330 nm. These
34 observations reveal diversity within the BCCR family and contribute to deeper understanding of
35 their independently evolved cation channel function.

36 IMPORTANCE

37 Cation channelrhodopsins, light-gated channels from flagellate green algae, are
38 extensively used as optogenetic photoactivators of neurons in research and recently have
39 progressed to clinical trials for vision restoration. However, the molecular mechanisms of their
40 photoactivation remain poorly understood. We recently identified cryptophyte cation
41 channelrhodopsins, structurally different from those of green algae, which have separately
42 evolved to converge on light-gated cation conductance. This study reveals diversity within this

Rapidly desensitizing cation channelrhodopsins

43 new protein family and describes a subclade with unusually rapid desensitization that results in
44 short transient photocurrents in continuous light. Such transient currents have not been observed
45 in the green algae channelrhodopsins and are potentially useful in optogenetic protocols. Kinetic
46 UV-vis spectroscopy and photoelectrophysiology reveal the desensitization is caused by rapid
47 accumulation of a non-conductive photointermediate in the photochemical reaction cycle. The
48 absorption maximum of the intermediate is 330 nm, the shortest wavelength reported in any
49 rhodopsin, indicating a novel chromophore structure.

50 INTRODUCTION

51 Channelrhodopsins are light-gated channels first discovered in green (chlorophyte)
52 flagellate algae, in which they serve as photoreceptors mediating phototaxis by depolarization of
53 the cell membrane (1-3). Currently, channelrhodopsins are widely used for control of neurons
54 and other excitable cells with light (“optogenetics”) (4) for research and also in clinical trials to
55 restore vision to the blind (5). Channelrhodopsins from chlorophyte algae conduct cations and
56 are therefore referred to as cation channelrhodopsins (CCRs). Anion-conducting
57 channelrhodopsins (ACRs) have been found in the phylogenetically distant cryptophyte algae (6)
58 and a second family more recently in environmental DNA samples of unidentified origin (7).
59 These three channelrhodopsin families share ~50% of overall sequence homology, including
60 several key residues shown to be required for their channel activity.

61 However, cryptophyte genomes also encode a family of microbial rhodopsins that show a
62 higher sequence homology to haloarchaeal proton-pumping rhodopsins than to any known
63 channelrhodopsins, and yet exhibit cation channel activity, apparently a product of convergent
64 evolution (8-10). In particular, these proteins contain homologs of the two carboxylate residues
65 that serve as the Schiff base proton acceptor and donor in *Halobacterium salinarum*

Rapidly desensitizing cation channelrhodopsins

66 bacteriorhodopsin (Asp85 and Asp96, respectively), which together with the Thr89 homolog
67 form the “DTD” motif characteristic of proton pumps. In contrast, in all other known
68 channelrhodopsins one or both of these positions are occupied by non-carboxylate residues.

69 Earlier we have shown that channel activity in CCRs 1 and 2 from the cryptophyte alga
70 *Guillardia theta* (*GtCCR1* and *GtCCR2*) is mechanistically distinct from that in chlorophyte
71 CCRs (9). According to our model, channel opening in these proteins requires deprotonation of
72 the Asp96 homolog and occurs >10-fold faster than reprotonation of the retinylidene Schiff base.
73 The latter is achieved by return of the proton from the earlier protonated acceptor, thus
74 preventing vectorial proton translocation across the membrane. To emphasize their distinction
75 from other known CCRs, we named these proteins “bacteriorhodopsin-like cation
76 channelrhodopsins” (BCCRs) (9).

77 Besides their fundamental importance as independently evolved light-gated cation
78 channels, BCCRs have attracted attention as optogenetic tools, because some of them exhibit
79 more red-shifted absorption enabling use of deeper penetrating long wavelength light and a
80 higher Na^+/H^+ permeability ratio favorable for neuron depolarization with minimal acidification
81 (8,11) compared to blue-light activated channelrhodopsin 2 from *Chlamydomonas reinhardtii*
82 (*CrChR2*), the molecule that so far has been most popular in optogenetic studies (12). Recently
83 ChRmine, a BCCR, has been used successfully to activate mouse neocortical neurons with
84 orange light (13).

85 Here we describe 19 BCCRs from 9 cryptophyte species, the protein sequences of which
86 form two separate branches (subfamilies) of the phylogenetic tree (Fig. 1A) in addition to that
87 comprising the previously characterized *GtCCR1* and *GtCCR2*. Two of these proteins derived
88 from two *Rhodomonas* species utilize a different activation mechanism and exhibit rapid

Rapidly desensitizing cation channelrhodopsins

89 desensitization of photocurrent under continuous illumination. We show that the photochemical
90 cycle of these channelrhodopsins involves accumulation of an extremely short-wavelength-
91 absorbing and long-living intermediate responsible for fast inactivation of their photocurrents.
92 These observations reveal diversity within the BCCR family and contribute to deeper
93 understanding of their cation channel function independently evolved from chlorophyte CCRs.

94 RESULTS

95 *Identification and electrophysiological screening of BCCR homologs*

96 Using probabilistic inference methods based on profile hidden Markov models (14) built
97 on previously known BCCR sequences from *G. theta*, we identified 19 new BCCR homologs
98 from nine marine cryptophyte strains included in the ongoing algal transcriptome sequencing
99 projects (15,16). The majority were cold-water species (from the Arctic or Antarctic), but
100 *Rhodomonas lens* was from the Gulf of Mexico and *R. salina*, from Milford, Connecticut. The
101 previously unclassified strain CCMP 2293 has recently been allocated to the new genus
102 *Baffinella* (as *B. frigidus*) (17).

103 Table 1 lists GenBank accession numbers, source organisms, transcript names, and
104 abbreviated protein names of the BCCR homologs identified in this study. In the abbreviated
105 protein names, the first two or three letters stand for the beginning letters of the genus and
106 species name. One of the sequences derived from *Rhodomonas lens* (*RICCR1*) exactly matched
107 the sequence recently reported under the name “ChRmine” and attributed to the marine ciliate
108 *Tiarina fusus* (13). As *T. fusus* culture used for RNA isolation was fed on *R. lens* (biosample
109 SAMN02740485), the presence of this sequence in the *T. fusus* transcriptome can be explained by
110 insufficient starvation of the organisms prior to RNA extraction.

Rapidly desensitizing cation channelrhodopsins

111 Fig. S1 shows protein alignment of the opsin domains of BCCRs identified in this study.
112 Asp85 and Thr89 (bacteriorhodopsin numbering) are conserved in all sequences, whereas Asp96
113 is replaced with Glu and Thr in *BfCCR2* and *G1CCR*, respectively. However, neither of these
114 sequences were electrogenic upon expression in mammalian cells (see below), and therefore the
115 functional importance of these substitutions could not be assessed. In many BCCR homologs the
116 position of bacteriorhodopsin's Arg82 is occupied by other residues (Lys, Ala, Pro, Gln or even
117 Glu (in *RaCCR2*)), which is unusual among microbial rhodopsins. Fig. 1A shows a phylogenetic
118 tree of the transmembrane domains of so far identified BCCRs. The previously characterized
119 *GtCCR1* and *GtCCR2*, together with *HpCCR*, a closely related sequence from *Hanusia phi*, form
120 a separate branch of this tree.

121 We synthesized human codon-optimized polynucleotides encoding the opsin domains of
122 19 newly identified BCCRs, fused them to an in-frame C-terminal EYFP (enhanced yellow
123 fluorescent protein) tag and expressed in HEK293 (human embryonic kidney) cells. Ten of the
124 encoded proteins generated photocurrents, the largest of which were the peak currents from
125 *RaCCR1* and *RsCCR1* (Fig. S2A). The action spectra were determined by measuring the initial
126 slopes of photocurrent in the linear range of the light intensity. The spectrum of *RaCCR1* closely
127 matched that of *R1CCR1* (also called ChRmine (13)) and peaked at ~530 nm; that of *RsCCR1*
128 was ~5 nm blue-shifted (Fig. S2B). The spectral maxima of other tested BCCRs are listed in
129 Table 1. The current kinetics was very diverse in the tested BCCRs. In particular, currents
130 recorded from *RaCCR1* and *RsCCR1* exhibited extremely rapid desensitization during
131 continuous illumination (Fig. 1B, red and blue lines, respectively). Representative photocurrent
132 traces from other tested BCCRs are shown in Fig. S3.

Rapidly desensitizing cation channelrhodopsins

133 To test relative permeability for Na⁺, we partially replaced this ion in the bath with non-
134 permeable *N*-methyl-D-glucamine (NMG⁺) and determined the reversal potentials (E_{rev}) by
135 measuring the current-voltage relationships in four BCCR variants that generated the largest
136 photocurrents. *RaCCR1* and *RsCCR1* showed large E_{rev} shifts towards the new equilibrium
137 potential for Na⁺ (Fig. S4A), similar to the earlier reported *GtCCR*s (9,10). However, *RaCCR2*
138 and *RsCCR2* showed smaller shifts, similar to that in *CrChR2* (18). When we reduced the bath
139 pH without changing its Na⁺ concentration, E_{rev} shifts were correspondingly smaller in *RaCCR1*
140 and *RsCCR1*, as compared to *RaCCR2* and *RsCCR2* (Fig. S4B), indicating a higher Na⁺/H⁺
141 permeability ratio of the former two CCRs, as compared to the latter. No change in E_{rev} was
142 detected upon partial replacement of Cl⁻ in the bath with bulky aspartate, indicating that neither
143 of the tested BCCRs conducted Cl⁻ (Fig. S4C).

144 *Absorption spectroscopy of RaCCR1 and RsCCR1*

145 To gain more insight into mechanisms of their photoactivation, we expressed and
146 detergent-purified *RaCCR1* and *RsCCR1* from the methylotrophic yeast *Pichia pastoris*. Their
147 absorption spectra in the visible range closely matched the action spectra of photocurrents with
148 main peaks at 530 and 524 nm, respectively (Fig. 2A). In addition, the absorption spectra of
149 dark-adapted *RaCCR1* and *RsCCR1* showed structured absorption in the near-UV range (with
150 peaks at ~307, 321 and 337 nm), in contrast to that of previously characterized *GtCCR2* purified
151 from the same expression host.

152 Similar UV bands had been reported in *GtCCR4* and tentatively attributed to impurities
153 of the sample (10). However, incubation of *RaCCR1* and *RsCCR1* with hydroxylamine, an agent
154 known to cleave the retinal chromophore from the bacteriorhodopsin apoprotein in a light-
155 dependent manner (19), decreased absorption in the UV region with the difference spectrum

Rapidly desensitizing cation channelrhodopsins

156 exhibiting the same triple-peak structure characteristic of protein-bound retinal (Fig. S5A and B).
157 In both proteins the rate of hydroxylamine bleaching of the UV bands was at least twice as fast
158 as that of the main band (Fig. S5C and D), indicating that the UV-absorbing fractions were more
159 accessible to hydroxylamine than the fractions absorbing in the visible range. Illumination
160 accelerated bleaching in the visible range, as expected for retinylidene proteins, but did not
161 influence the rate of bleaching at 321 nm (Fig. S5C and D). These results suggest that the
162 structured UV absorbance in the dark-adapted sample is attributable to retinal binding to partially
163 misfolded *RaCCR1* and *RsCCR1*. The ratio of the UV absorption to the main peak absorption
164 varied from 0.4 to 1.5 in different preparations, did not depend on the length of the expression
165 construct, purification procedure, or storage conditions, and may reflect the relative amount of
166 misfolded protein.

167 Continuous illumination of detergent-purified *RaCCR1* with visible light decreased
168 absorption at the main band (P530) and led to formation of a product (P330) with structured
169 absorption in the UV region with three peaks at 318, 330 and 346 nm (Fig. 2B), red-shifted from
170 those observed in the dark. Dissipation of P330 occurred on the time scale of seconds in parallel
171 with recovery of the unphotolyzed state P530 (Fig. 2C). The recovery of the unphotolyzed state
172 was ~3-fold slower in *Pichia* membranes than in detergent-purified protein (Fig. S6A). A very
173 similar product with structured UV absorption was also formed upon illumination of purified
174 *RsCCR1* (Fig. S6B), with a rate of dissipation in the dark >2-fold faster than that in *RaCCR1*
175 (Fig. 2D).

176 *Mechanism of photocurrent desensitization*

177 As described above, photocurrents from *RaCCR1* and *RsCCR1* exhibited rapid
178 desensitization under continuous light (Fig. 1B). Desensitization was also observed under

Rapidly desensitizing cation channelrhodopsins

179 stimulation with 6-ns laser flashes at 0.1 Hz frequency even at 10% power (Fig. S6C), which
180 argues against its origin from a secondary photochemical process. An alternative explanation for
181 photocurrent desensitization is the existence of a long-lived non-conductive state in the single-
182 turnover photocycle. To determine the rate of peak current recovery, a second flash was applied
183 after a variable time delay. The rate of restoration of the ability to generate electric current
184 closely matched that of P330 dissipation in both purified proteins (Fig. 2D), strongly suggesting
185 that accumulation of P330 is responsible for the rapid desensitization of photocurrents generated
186 by *RaCCR1* and *RsCCR1*.

187 Fig. S7A shows a series of photocurrent traces generated by *RaCCR1* in response to 1-s
188 light pulses of different intensities. The peak photocurrent increased over the entire tested
189 intensity range, whereas the degree of desensitization reached saturation two orders of magnitude
190 earlier (Fig. S7B), and similar results were obtained with *RsCCR1* (Fig. S7C). These
191 observations show that the long-lived non-conductive P330 is not in equilibrium with the
192 unphotolyzed state of the protein.

193 Alkalization caused formation of a UV-absorbing species of *RaCCR1* with a structured
194 spectrum closely matching that of the form obtained by illumination (Fig. 3A). The pK_a of this
195 process was identical to that of decrease of absorbance at 530 nm, which showed that the UV-
196 absorbing species was produced from P530 (Fig. 3B). The alkali-induced conversion of the
197 unphotolyzed form absorbing at 530 nm to P330 decreased the amplitude of the photo-induced
198 conversion. When illuminated *RaCCR1* samples were incubated in the dark at high pH, only a
199 small decrease in absorbance at 330 nm was observed, as compared to neutral pH conditions
200 (Fig. 3C). The pK_a of this decrease in amplitude was identical to that of conversion of P530 to
201 the UV-absorbing species (Fig. 3D). We conclude from these observations that the same species

Rapidly desensitizing cation channelrhodopsins

202 accumulated at high pH as that obtained by illumination (i.e. P330). To the best of our
203 knowledge, P330 is the shortest wavelength intermediate observed in the photocycle of any
204 microbial rhodopsin. In addition to formation of P330, alkalization caused accumulation of an
205 M-like intermediate absorbing at ~ 390 nm with $pK_a \sim 9.0$, although its concentration (assuming
206 \sim equal extinction coefficients) was 10-fold smaller than that of P330 (Fig. 3E).

207 At pH 10 essentially all molecules were converted from the unphotolysed form to P330.
208 This allowed us to use FT-Raman spectroscopy to probe its chromophore structure in the dark.
209 The Raman spectra measured at pH 7.2 and 10 and their difference spectrum are shown in Fig.
210 3F. The main ethylenic C=C stretch at 1530 cm^{-1} , which corresponds to the main visible peak at
211 530 nm (20), and the fingerprint C-C stretches at 1200 and 1163 cm^{-1} showed that at pH 7.2
212 retinal was predominantly in an all-*trans* configuration. Upon alkalization the band at 1530 cm^{-1}
213 was strongly reduced, and new bands appeared at 1590 cm^{-1} and 1562 cm^{-1} which presumably
214 corresponded, respectively, to P330 and the M-like intermediate absorbing at ~ 390 nm. The
215 same two bands were clearly resolved in the difference spectrum.

216 *Fast photochemical conversions*

217 Fast photochemical conversions in the near UV and visible range were analyzed by flash
218 photolysis. Fig. S8A shows a series of absorption changes in *RsCCR1* detected at wavelengths
219 from 390 to 570 nm at 10-nm increments. Only negligible (less than 0.5 mOD) oppositely
220 directed components with the time constant (τ) values ~ 60 -100 μs were observed at the
221 wavelengths at which maximal absorption of the red-shifted K and blue-shifted L intermediates
222 are expected (480 and 560 nm, respectively) (Fig. S8B). Therefore we could not follow the K to
223 L transition, which occurred on a much faster time scale. To obtain the spectral changes due to L
224 formation, we plotted the mean absorption changes in the time window between 50 and 100 μs

Rapidly desensitizing cation channelrhodopsins

225 after the flash against wavelength (Fig. 4A). The maximum of the L intermediate in this
226 difference spectrum was at ~460 nm.

227 The spectral characteristics of the later transitions were obtained by global fit analysis.
228 The appearance of a typical M intermediate with the absorption maximum at ~390 nm (the
229 positive peak in Fig. 4B) was observed within 1 ms. After that, biphasic bleaching at all visible
230 wavelengths took place, which was obviously related to generation of P330 form. Fast bleaching
231 with $\tau \sim 4.5$ ms reflected the decay of the bulk of the initial form and may involve the appearance
232 of a blue-absorbing (N?) intermediate (Fig. 4C), which was more obvious during the slow
233 bleaching with $\tau \sim 40$ ms (Fig. 4D). The recovery of the initial state proceeded in two steps with τ
234 1.4 and 3.8 s. At least the fast recovery involved depletion of a blue-absorbing intermediate (Fig.
235 4E). The τ of the main slow recovery component was equal to those of P330 dissipation and
236 restoration of electrical sensitivity (Fig. 4F and Fig. 2D). Qualitatively similar phototransitions
237 were observed in the second pigment *RaCCR1* with time constants of components 0.3, 6, 40,
238 3200 and 1140 ms (Fig. S9). In agreement with slower dissipation of the P330 intermediate and
239 restoration of light sensitivity in this pigment as compared to *RsCCR1* (Fig. 2D), the recovery in
240 the visible range was also slower, and depletion of the blue absorbing form was also observed
241 (Fig. S9E and F). However, the 40-ms component which in *RsCCR1* corresponded to slow
242 bleaching, in *RaCCR1* revealed fast recovery.

243 We recorded photocurrents in HEK cells upon 6-ns laser flash excitation at 532 nm as in
244 flash-photolysis measurements for kinetic comparison with absorption changes in purified
245 proteins. Channel opening and closing in *RaCCR1* and *RsCCR1* took place in the same time
246 windows as absorption changes at the wavelengths of M-intermediate absorption in which proton
247 transfers occur (Fig. 5A and B).

Rapidly desensitizing cation channelrhodopsins

248 In the current traces generated by *GtCCR1* and *GtCCR2*, a large peak was observed in
249 the 30-100 μ s time domain prior to channel opening (9). This peak, also exhibited by some low-
250 efficiency CCRs from green algae, reflects intramolecular transfer of the Schiff base proton to an
251 outwardly located acceptor, integrated by the measuring system (21). This component could also
252 be resolved in the current traces from *RaCCR1* and *RsCCR1* recorded at the voltages near the
253 reversal potential for Na^+ , but it was \sim 100-fold smaller than that in *GtCCR1* and *GtCCR2* (Fig.
254 S10).

255 *Mutagenesis analysis*

256 In *GtCCR1* and *GtCCR2* we found that a neutralizing mutation of the Asp96 homolog
257 (Asp98) completely suppressed channel activity, so that only intramolecular transfer of the
258 Schiff base proton could be detected (9). The corresponding D125N and D128N mutations in
259 *RaCCR1* and *RsCCR1*, respectively, did not eliminate channel currents (Fig. 6A). Neutralization
260 of the Asp85 homolog in *RaCCR1* (the D114N mutation) reduced expression of the construct, as
261 judged by the tag fluorescence, and no photocurrents above the noise level could be detected.
262 Replacement of Cys119 (corresponding to Thr90 in bacteriorhodopsin) with Ala completely
263 abolished photocurrents in *RaCCR1*, as did also the corresponding mutations in *RaCCR2*,
264 *GtCCR2* and *PsuCCR*. In the *RaCCR1_C119T* mutant the photocurrent amplitude was greatly
265 reduced (the mean peak current in response to a first light pulse of maximal intensity was 10 ± 3
266 pA, $n = 14$ cells). These tiny currents, however, exhibited only \sim 40% desensitization during 1-s
267 continuous illumination (Fig. 6B), i.e., much less than in the wild type. The photocurrent decay
268 after switching the light off was biphasic, with the slow phase on the second time scale. But the
269 most striking difference of this mutant from the wild type was the absence of the long-living UV-
270 absorbing form with the structured spectrum corresponding to P330 in the wild type (Fig. 6C).

Rapidly desensitizing cation channelrhodopsins

271 Instead, a smooth peak with the maximum at 380 nm (the M state) was produced. The dissipation
272 of this state and the recovery of the unphotolyzed state with the peak absorbance at 506 nm were
273 very slow (Fig. 6D).

274 DISCUSSION

275 Our results show that BCCRs are widely spread among cryptophyte algae and form three
276 branches (subfamilies) of a phylogenetic tree. BCCRs exhibit diverse current kinetics, spectral
277 sensitivity and Na⁺/H⁺ permeability ratios, as has also been found in other channelrhodopsin
278 families. Two representatives of the currently studied BCCRs differ in their mechanism of
279 photoactivation from previously described *GtCCR1* and 2, which belong to a different subfamily
280 of cryptophyte CCRs. Most notably, a particular proton transfer essential to trigger channel
281 opening in the earlier reported subfamily is not required in the subfamily described in this study.
282 Photocurrents by *RaCCR1* and *RsCCR1* exhibit very rapid desensitization under continuous
283 illumination, which we show is related to the formation of a long-living UV-absorbing
284 intermediate in their photocycles. Similar rapid photocurrent desensitization was observed in
285 anion-conducting MerMAIDs, explained by accumulation of a long-lived M intermediate with an
286 unusual short-wavelength maximum absorption peak at 364 nm (7). In both *RaCCR1* and
287 *RsCCR1* two distinct UV-absorbing intermediates were accumulated upon illumination, one at
288 390 nm, typical of M intermediates, and the other a triple-peaked species with a uniquely far
289 blue-shifted spectrum with a 330-nm maximum.

290 Flash photolysis measurements revealed an extremely fast (<1 μs after the flash)
291 appearance of the L intermediate that might be in equilibrium with K during the first 100 μs in
292 *RaCCR1* and *RsCCR1*. The typical M intermediate absorbing at 390 nm was formed during 0.1-
293 1 ms. We could not follow the appearance of the second blue-shifted intermediate (P330)

Rapidly desensitizing cation channelrhodopsins

294 because the low signal-to-noise ratio in the near UV range limited measurements to wavelengths
295 ≥ 380 nm. However, we observed bleaching in the entire visible range on the millisecond time
296 scale, which likely indicated accumulation of P330. A decrease of absorption in the blue range
297 was observed during the fast recovery of the unphotolyzed states of both *RaCCR1* and *RsCCR1*.
298 This most probably reflects dissipation of an N-like intermediate that appears earlier in the
299 photocycle.

300 The short-wavelength absorption of photointermediate P330 is unique among
301 photocycles of microbial rhodopsins. The extremely short wavelength absorption and very high
302 ethylenic stretch wavenumber of a corresponding band in Raman spectra suggest an extremely
303 hydrophobic environment of the retinal moiety. The chromophore in P330 could be, for example,
304 retro-retinal, a derivative in which all double bonds are shifted towards the ring by one position
305 (22), or a free retinal that remains in the binding pocket (23). A linear photocycle involving P330
306 is the simplest scheme that fits our results; however, we cannot exclude a branched photocycle as
307 was proposed for the *CrChR2_C128T* mutant (22).

308 Rapid desensitization observed in *RaCCR1* and *RsCCR1* under continuous illumination
309 would potentially allow temporally precise neuronal activation even in the presence of light that
310 can be used for fluorescent imaging. Additional advantages of these two BCCRs are their
311 relatively red-shifted absorption and high Na^+/H^+ permeability ratio. Better understanding of
312 their molecular mechanisms will facilitate their rational design for optogenetic needs.

313 MATERIALS AND METHODS

314 *Bioinformatics*

Rapidly desensitizing cation channelrhodopsins

315 BCCR homologs were identified by searching cryptophyte transcriptomes from the
316 MMETS sequencing project (15) and 1KP project (16) using probabilistic inference methods
317 based on profile hidden Markov models (profile HMMs). Profile HMMs were built from
318 previously known BCCR sequences using HMMER software (version 3.1b2; (14)) with default
319 parameters and refined upon functional testing of the homologs by patch clamping. Search
320 procedures were automated with Python 2.7 and the Biopython module (24). The protein
321 sequence alignment was created using MUSCLE algorithm implemented in DNASTAR
322 Lasergene (Madison, WI) MegAlign Pro software. The phylogenetic tree was visualized using
323 Dendroscope software (25).

324 *Molecular biology*

325 For expression in HEK293 cells, DNA polynucleotides encoding the BCCR opsin
326 domains optimized for human codon usage were synthesized (GenScript, Piscataway, NJ) and
327 cloned into the mammalian expression vector pcDNA3.1 (Life Technologies, Grand Island, NY)
328 in frame with an EYFP tag. For expression in *Pichia*, the opsin-encoding constructs were fused
329 in frame with a C-terminal eight-His tag and subcloned into the pPIC9K vector (Invitrogen).
330 Mutants were generated with Quikchange XL kit (Agilent Technologies, Santa Clara, CA) and
331 verified by sequencing.

332 *HEK293 transfection and patch clamp recording*

333 HEK293 cells were transfected using the ScreenFectA transfection reagent (Waco
334 Chemicals USA, Richmond, VA). All-*trans*-retinal (Sigma) was added at the final concentration
335 of 3 μ M immediately after transfection. Photocurrents were recorded 48-96 h after transfection
336 in the whole-cell voltage clamp mode with an Axopatch 200B amplifier (Molecular Devices,

Rapidly desensitizing cation channelrhodopsins

337 Union City, CA) using the 10 kHz low-pass Bessel filter. The signals were digitized with a
338 Digidata 1440A using pClamp 10 software (both from Molecular Devices). Patch pipettes with
339 resistances of 2-4 M Ω were fabricated from borosilicate glass. The standard pipette solution
340 contained (in mM): KCl 126, MgCl₂ 2, CaCl₂ 0.5, Na-EGTA 5, HEPES 25, pH 7.4. The standard
341 bath solution contained (in mM): NaCl 150, CaCl₂ 1.8, MgCl₂ 1, glucose 5, HEPES 10, pH 7.4.
342 A 4 M KCl bridge was used in all experiments, and possible diffusion of Cl⁻ from the bridge to
343 the bath was minimized by frequent replacement of the bath solution with fresh buffer. For
344 measurements of the reversal potential shifts under varied ionic conditions, Na⁺ was substituted
345 for K⁺ in the pipette solution to minimize the number of ionic species in the system. To reduce
346 the Cl⁻ concentration in the bath, NaCl was replaced with Na-aspartate; to reduce the Na⁺
347 concentration, with N-methyl-D-glucamine chloride; to increase the H⁺ concentration, pH was
348 adjusted with H₂SO₄. The holding voltages were corrected for liquid junction potentials
349 calculated using the Clampex built-in LJP calculator (26). Continuous light pulses were provided
350 by a Polychrome V light source (T.I.L.L. Photonics GMBH, Grafelfing, Germany) in
351 combination with a mechanical shutter (Uniblitz Model LS6, Vincent Associates, Rochester,
352 NY; half-opening time 0.5 ms). The maximal quantum density at the focal plane of the 40 \times
353 objective was 7.7 mW mm⁻² at 515 nm. The action spectra were constructed by calculation of the
354 initial slope of photocurrent and corrected for the quantum density measured at each wavelength.
355 Laser excitation was provided by a Minilite Nd:YAG laser (532 nm, pulsewidth 6 ns, energy 12
356 mJ; Continuum, San Jose, CA). The current traces were logarithmically filtered using a custom
357 software, and the laser artifact was digitally subtracted. Curve fitting was performed by Origin
358 Pro software (OriginLab Corporation, Northampton, MA).

359 *Expression and purification of BCCRs from Pichia*

Rapidly desensitizing cation channelrhodopsins

360 The plasmids encoding BCCRs were linearized with SallI and used to transform *P.*
361 *pastoris* strain SMD1168 (*his4*, *pep4*) by electroporation. Transformants were first screened for
362 their ability to grow on histidine-deficient medium, and second, for their geneticin resistance.
363 Single colonies that grew on 4 mg/ml geneticin were screened by small-scale cultivation, and
364 clones of the brightest color were selected. For protein purification, a starter culture was
365 inoculated into buffered complex glycerol medium until A600 reached 4–8, after which the cells
366 were harvested by centrifugation at 5000 rpm and transferred to buffered complex methanol
367 medium supplemented with 5 μ M all-*trans* retinal (Sigma Aldrich). Expression was induced by
368 the addition of 0.5% methanol. After 24–30 h, the cells were harvested and disrupted in a bead
369 beater (BioSpec Products, Bartlesville, OK) in buffer A (20 mM sodium phosphate, pH 7.4, 100
370 mM NaCl, 1 mM EDTA, 5% glycerol). After removing cell debris by low-speed centrifugation,
371 membrane fragments were collected by ultracentrifugation at 40,000 rpm in a Ti45 rotor,
372 resuspended in buffer B (20 mM Hepes, pH 7.4, 300 mM NaCl, 5% glycerol) and solubilized by
373 incubation with 1.5% dodecyl maltoside (DDM) for 1.5 h or overnight at 4°C. Non-solubilized
374 material was removed by ultracentrifugation at 50,000 rpm in a TLA-100 rotor. The supernatant
375 was mixed with nickel-nitrilotriacetic acid agarose beads (Qiagen, Hilden, Germany) and loaded
376 on a column. The proteins were eluted with buffer C (20 mM Hepes, pH 7.4, 300 mM NaCl, 5%
377 glycerol, 0.02% DDM) containing 300 mM imidazole. The pigments were concentrated and
378 imidazole was removed by repetitive washing with imidazole-free buffer C using YM-10
379 centrifugal filters (Amicon, Billerica, MA).

380 *Absorption spectroscopy and flash photolysis*

381 Absorption spectra of purified BCCRs were recorded using a Cary 4000
382 spectrophotometer (Varian, Palo Alto, CA). The pK_a was determined by fitting the classical

Rapidly desensitizing cation channelrhodopsins

383 Henderson-Hasselbalch equation in the form $y = A/(1+10E(pK_a-pH))$ to experimental data.
384 Light-induced absorption changes were measured with a laboratory-constructed crossbeam
385 apparatus. Excitation flashes (532 nm, 6 ns, 40 mJ) were provided by a Surelite I Nd-YAG laser
386 (Continuum, Santa Clara, CA). Measuring light was from a 250-W incandescent tungsten lamp
387 combined with a McPherson monochromator (model 272, Acton, MA). Absorption changes were
388 detected with a Hamamatsu Photonics (Bridgewater, NJ) photomultiplier tube (model R928),
389 protected from excitation laser flashes by a second monochromator of the same type. Signals
390 were amplified by a low noise current amplifier (model SR445A; Stanford Research Systems,
391 Sunnyvale, CA) and digitized with a GaGe Octopus digitizer board (model CS8327,
392 DynamicSignals LLC, Lockport, IL), maximum sampling rate 50 MHz. Logarithmic filtration of
393 the data was performed using the GageCon program (27).

394 *Fourier-transformed Raman spectroscopy*

395 Fourier-transformed Raman spectra were collected in 5 μ l of a concentrated detergent-
396 solubilized protein in pH-adjusted elution buffer placed in a metallic holder and covered by
397 adhesive tape. The scattering was recorded in 180° backscattering geometry, using FRA106/s
398 accessory to the Bruker IFS66vs spectrometer, with Nd-YAG laser excitation provided at 1064
399 nm, at a 2 cm^{-1} resolution, controlled by the OPUS software. At least 10000 scans averaged per
400 sample. Raman spectra of the buffers were taken separately in the same geometry and subtracted
401 to get pure protein spectra.

402 *Statistics*

403 Descriptive statistics was used as implemented in Origin software. The data are presented
404 as mean \pm s.e.m. values; the data from individual replicates are also shown when appropriate.

Rapidly desensitizing cation channelrhodopsins

405 The sample size was estimated from previous experience and published work on similar subjects,
406 as recommended by the NIH guidelines (28).

407 *Data availability*

408 The polynucleotide sequences of BCCR homologs reported in this study have been
409 deposited to GenBank (accession numbers MN585290-MN585308).

410 **Acknowledgements**

411 We thank Olivier Morelle for technical assistance with bioinformatics analysis. This
412 work was supported by National Institutes of Health Grant R01GM027750, the Hermann Eye
413 Fund, and Endowed Chair AU-0009 from the Robert A. Welch Foundation to J.L.S, and by the
414 Natural Sciences and Engineering Research Council of Canada (NSERC) Discovery Grant
415 RGPIN-2018-04397 to L.S.B. The content is solely the responsibility of the authors and does not
416 necessarily represent the official views of the National Institutes of Health.

417 **Conflict of interest**

418 The authors declare that they have no conflicts of interest with the contents of this article.

419 **REFERENCES**

- 420 1. Sineshchekov, O. A., Jung, K.-H., and Spudich, J. L. (2002) Two rhodopsins mediate
421 phototaxis to low- and high-intensity light in *Chlamydomonas reinhardtii*. *Proc. Natl.*
422 *Acad. Sci. USA* 99, 8689-8694
- 423 2. Nagel, G., Ollig, D., Fuhrmann, M., Kateriya, S., Musti, A. M., Bamberg, E., and
424 Hegemann, P. (2002) Channelrhodopsin-1: a light-gated proton channel in green algae.
425 *Science* 296, 2395-2398

Rapidly desensitizing cation channelrhodopsins

- 426 3. Nagel, G., Szellas, T., Huhn, W., Kateriya, S., Adeishvili, N., Berthold, P., Ollig, D.,
427 Hegemann, P., and Bamberg, E. (2003) Channelrhodopsin-2, a directly light-gated
428 cation-selective membrane channel. *Proc. Natl. Acad. Sci. USA* 100, 13940-13945
- 429 4. Deisseroth, K. (2011) Optogenetics. *Nat. Methods* 8, 26-29
- 430 5. Vazquez-Dominguez, I., Garanto, A., and Collin, R. W. J. (2019) Molecular therapies for
431 inherited retinal diseases - Current standing, opportunities and challenges. *Genes (Basel)*
432 10
- 433 6. Govorunova, E. G., Sineshchekov, O. A., Liu, X., Janz, R., and Spudich, J. L. (2015)
434 Natural light-gated anion channels: A family of microbial rhodopsins for advanced
435 optogenetics. *Science* 349, 647-650
- 436 7. Oppermann, J., Fischer, P., Silapetere, A., Liepe, B., Rodriguez-Rozada, S., Flores-Uribe,
437 J., Peter, E., Keidel, A., Vierock, J., Kaufmann, J., Broser, M., Luck, M., Bartl, F.,
438 Hildebrandt, P., Simon Wiegert, J., Beja, O., Hegemann, P., and Wietek, J. (2019)
439 MerMAIDs: a family of metagenomically discovered marine anion-conducting and
440 intensely desensitizing channelrhodopsins. *Nat. Commun.* 10, 3315
- 441 8. Govorunova, E. G., Sineshchekov, O. A., and Spudich, J. L. (2016) Structurally distinct
442 cation channelrhodopsins from cryptophyte algae. *Biophys. J.* 110, 2302-2304
- 443 9. Sineshchekov, O. A., Govorunova, E. G., Li, H., and Spudich, J. L. (2017)
444 Bacteriorhodopsin-like channelrhodopsins: Alternative mechanism for control of cation
445 conductance. *Proc. Natl. Acad. Sci. USA* 114, E9512-E9519
- 446 10. Yamauchi, Y., Konno, M., Ito, S., Tsunoda, S. P., Inoue, K., and Kandori, H. (2017)
447 Molecular properties of a DTD channelrhodopsin from *Guillardia theta*. *Biophys.*
448 *Physicobiol.* 14, 57-66

Rapidly desensitizing cation channelrhodopsins

- 449 11. Shigemura, S., Hososhima, S., Kandori, H., and Tsunoda, S. P. (2019) Ion channel
450 properties of a cation channelrhodopsin, Gt_CCR4. *Appl. Sci.* 9, 3440
- 451 12. Wietek, J., and Prigge, M. (2016) Enhancing channelrhodopsins: An overview. *Methods*
452 *Mol. Biol.* 1408, 141-165
- 453 13. Marshel, J. H., Kim, Y. S., Machado, T. A., Quirin, S., Benson, B., Kadmon, J., Raja, C.,
454 Chibukhchyan, A., Ramakrishnan, C., Inoue, M., Shane, J. C., McKnight, D. J.,
455 Yoshizawa, S., Kato, H. E., Ganguli, S., and Deisseroth, K. (2019) Cortical layer-specific
456 critical dynamics triggering perception. *Science*
- 457 14. Eddy, S. R. (2011) Accelerated profile HMM searches. *PLoS Comput. Biol.* 7, e1002195
- 458 15. Keeling, P. J., Burki, F., Wilcox, H. M., Allam, B., Allen, E. E., Amaral-Zettler, L. A.,
459 Armbrust, E. V., Archibald, J. M., Bharti, A. K., Bell, C. J., Beszteri, B., Bidle, K. D.,
460 Cameron, C. T., Campbell, L., Caron, D. A., Cattolico, R. A., Collier, J. L., Coyne, K.,
461 Davy, S. K., Deschamps, P., Dyrman, S. T., Edvardsen, B., Gates, R. D., Gobler, C. J.,
462 Greenwood, S. J., Guida, S. M., Jacobi, J. L., Jakobsen, K. S., James, E. R., Jenkins, B.,
463 John, U., Johnson, M. D., Juhl, A. R., Kamp, A., Katz, L. A., Kiene, R., Kudryavtsev, A.,
464 Leander, B. S., Lin, S., Lovejoy, C., Lynn, D., Marchetti, A., McManus, G., Nedelcu, A.
465 M., Menden-Deuer, S., Miceli, C., Mock, T., Montresor, M., Moran, M. A., Murray, S.,
466 Nadathur, G., Nagai, S., Ngam, P. B., Palenik, B., Pawlowski, J., Petroni, G., Piganeau,
467 G., Posewitz, M. C., Rengefors, K., Romano, G., Rumpho, M. E., Rynearson, T.,
468 Schilling, K. B., Schroeder, D. C., Simpson, A. G., Slamovits, C. H., Smith, D. R., Smith,
469 G. J., Smith, S. R., Sosik, H. M., Stief, P., Theriot, E., Twary, S. N., Umale, P. E., Vaultot,
470 D., Wawrik, B., Wheeler, G. L., Wilson, W. H., Xu, Y., Zingone, A., and Worden, A. Z.
471 (2014) The Marine Microbial Eukaryote Transcriptome Sequencing Project (MMETSP):

Rapidly desensitizing cation channelrhodopsins

- 472 illuminating the functional diversity of eukaryotic life in the oceans through
473 transcriptome sequencing. *PLoS Biol.* 12, e1001889
- 474 16. Matasci, N., Hung, L. H., Yan, Z., Carpenter, E. J., Wickett, N. J., Mirarab, S., Nguyen,
475 N., Warnow, T., Ayyampalayam, S., Barker, M., Burleigh, J. G., Gitzendanner, M. A.,
476 Wafula, E., Der, J. P., dePamphilis, C. W., Roure, B., Philippe, H., Ruhfel, B. R., Miles,
477 N. W., Graham, S. W., Mathews, S., Surek, B., Melkonian, M., Soltis, D. E., Soltis, P. S.,
478 Rothfels, C., Pokorny, L., Shaw, J. A., DeGironimo, L., Stevenson, D. W., Villarreal, J.,
479 C., Chen, T., Kutchan, T. M., Rolf, M., Baucom, R. S., Deyholos, M. K., Samudrala, R.,
480 Tian, Z., Wu, X., Sun, X., Zhang, Y., Wang, J., Leebens-Mack, J., and Wong, G. K.
481 (2014) Data access for the 1,000 Plants (1KP) project. *Gigascience* 3, 17
- 482 17. Daugbjerg, N., Norlin, A., and Lovejoy, C. (2018) *Baffinella frigidus* gen. et sp. nov.
483 (*Baffinellaceae* fam. nov., *Cryptophyceae*) from Baffin Bay: Morphology, pigment
484 profile, phylogeny, and growth rate response to three abiotic factors. *J. Phycol.* 54, 665-
485 680
- 486 18. Govorunova, E. G., Sineshchekov, O. A., Li, H., Janz, R., and Spudich, J. L. (2013)
487 Characterization of a highly efficient blue-shifted channelrhodopsin from the marine alga
488 *Platymonas subcordiformis*. *J. Biol. Chem.* 288, 29911-29922
- 489 19. Oesterhelt, D., Gruber, H., and Schuhmann, L. (1974) Light-dependent reaction of
490 bacteriorhodopsin with hydroxylamine in cell suspensions of *Halobacterium halobium*:
491 demonstration of an apomembrane. *FEBS Lett.* 44
- 492 20. Kakitani, H., Kakitani, T., Rodman, H., Honig, B., and Callender, R. (1983) Correlation
493 of vibrational frequencies with absorption maxima in polyenes, rhodopsin,
494 bacteriorhodopsin, and retinal analogs. *J. Phys. Chem.* 87, 3620-3628

Rapidly desensitizing cation channelrhodopsins

- 495 21. Sineshchekov, O. A., Govorunova, E. G., Wang, J., Li, H., and Spudich, J. L. (2013)
496 Intramolecular proton transfer in channelrhodopsins. *Biophys. J.* 104, 807-817
- 497 22. Stehfest, K., Ritter, E., Berndt, A., Bartl, F., and Hegemann, P. (2010) The branched
498 photocycle of the slow-cycling channelrhodopsin-2 mutant C128T. *J. Mol. Biol.* 398,
499 690-702
- 500 23. Bruun, S., Naumann, H., Kuhlmann, U., Schulz, C., Stehfest, K., Hegemann, P., and
501 Hildebrandt, P. (2011) The chromophore structure of the long-lived intermediate of the
502 C128T channelrhodopsin-2 variant. *FEBS Lett.*
- 503 24. Cock, P. J., Antao, T., Chang, J. T., Chapman, B. A., Cox, C. J., Dalke, A., Friedberg, I.,
504 Hamelryck, T., Kauff, F., Wilczynski, B., and de Hoon, M. J. (2009) Biopython: freely
505 available Python tools for computational molecular biology and bioinformatics.
506 *Bioinformatics* 25, 1422-1423
- 507 25. Huson, D. H., and Scornavacca, C. (2012) Dendroscope 3: an interactive tool for rooted
508 phylogenetic trees and networks. *Syst. Biol.* 61, 1061-1067
- 509 26. Barry, P. H. (1994) JPCalc, a software package for calculating liquid junction potential
510 corrections in patch-clamp, intracellular, epithelial and bilayer measurements and for
511 correcting junction potential measurements. *J. Neurosci. Methods* 51, 107-116
- 512 27. Waschuk, S. A., Bezerra, A. G. J., Shi, L., and Brown, L. S. (2005) Leptosphaeria
513 rhodopsin: Bacteriorhodopsin-like proton pump from a eukaryote. *Proc. Natl. Acad. Sci.*
514 *USA* 102, 6879-6883
- 515 28. Dell, R. B., Holleran, S., and Ramakrishnan, R. (2002) Sample size determination. *ILAR*
516 *J.* 43, 207-213

517 FIGURE LEGENDS

Rapidly desensitizing cation channelrhodopsins

518 **Figure 1.** (A) A phylogenetic tree of BCCR transmembrane domains. Bold font shows the
519 proteins that generated photocurrents upon expression in mammalian cells. (B) Normalized
520 photocurrent traces from *RaCCR1* and *RsCCR1* (colored lines) recorded at -60 mV in response
521 to a light pulse, duration of which is shown as the bar on top. Traces from previously
522 characterized *GtCCR1* and *GtCCR2* (black lines) are shown for comparison.

523 **Figure 2.** (A) The absorption spectra of dark-adapted detergent-purified proteins. (B) The
524 difference (light minus dark) absorption spectrum of *RaCCR1*. (C) The time course of absorption
525 changes at 330 and 530 nm during dark incubation of illuminated *RaCCR1*. (D) The time course
526 of absorption changes at 330 nm in *RsCCR1* (that in *RaCCR1* from panel C is shown for
527 comparison) and photocurrent recovery for both channelrhodopsins.

528 **Figure 3.** (A) The UV region of the difference absorption spectra of *RaCCR1* obtained upon a
529 pH increase from 7.2 to 9.3 (red, left axis) or upon illumination (black, right axis). (B) The pH
530 dependence of absorbance changes at 330 nm (black, left axis) and 530 nm (red, right axis). (C)
531 Absorbance changes at 330 nm during incubation of *RaCCR1* in the dark at the indicated pH.
532 (D) The pH dependence of the light-induced absorbance changes at 330 nm. (E) The difference
533 absorption spectrum pH 10 minus pH 7.2. (F) The FT-Raman spectra measured at pH 7.2 and 10,
534 and their difference spectrum.

535 **Figure 4.** (A) Mean photoinduced absorbance changes recorded from purified *RsCCR1* in the
536 50-100 μ s time window. (B-F) Spectral transitions in *RsCCR1* derived by global fit analysis.

537 **Figure 5.** (A and B) Laser flash-evoked photocurrents at -60 mV (red) and photoinduced
538 absorbance change (blue) recorded from *RaCCR1* (A) and *RsCCR1* (B).

Rapidly desensitizing cation channelrhodopsins

539 **Figure 6.** (A) Laser-evoked photocurrents recorded at -60 mV from the mutants of the Asp96
540 homolog in three BCCR mutants in which the homolog of Asp96 was neutralized. (B) The
541 current trace recorded in response to 1-s light pulse from the *RaCCR1_C119T* mutant (red line).
542 The normalized trace from the wild type is shown in black for comparison. (C) The light minus
543 dark absorption spectrum of purified *RaCCR1_C119T* mutant (red). The spectrum for the wild
544 type is shown in black for comparison. (D) Absorbance changes in purified illuminated
545 *RaCCR1_C119T* during incubation in the dark.

546 SUPPLEMENTARY FIGURE LEGENDS

547 **Figure S1.** Protein sequence alignment of the opsin domains of BCCRs first reported in this
548 study. Residues are color-coded according to their chemical properties.

549 **Figure S2.** (A) Amplitudes of BCCR photocurrents recorded at -60 mV at the amplifier output
550 upon photostimulation at the peak sensitivity wavelength. Stationary currents were measured at
551 the end of a 1-s light pulse. The data are the mean values \pm sem recorded from 3-24 individual
552 cells. The data from individual cells are shown as empty diamonds. (B) The action spectra of
553 photocurrents. The data are the mean values \pm sem recorded from 6-8 individual scans.

554 **Figure S3.** Representative photocurrent traces recorded from indicated BCCRs at -60 mV at the
555 amplifier output in response to a light pulse, the duration of which is shown as a colored bar on
556 top.

557 **Figure S4.** (A-C) The reversal potentials measured under indicated ionic conditions. The data
558 points are the mean values \pm sem. The data from individual cells are shown as empty diamonds.

Rapidly desensitizing cation channelrhodopsins

559 **Figure S5.** (A and B) The difference spectra (treated minus untreated sample) obtained by
560 incubation of indicated proteins with hydroxylamine (HA) in the dark (black lines) and under
561 illumination (red lines). (C and D) The time course of hydroxylamine bleaching of the UV and
562 visible absorption bands. The bar on top shows the time of illumination.

563 **Figure S6.** (A) The rate of absorbance recovery at 530 nm of *RaCCR1* in *Pichia* membranes (red
564 line) as compared to that in detergent (black line). (B) The UV portion of the *RsCCR1* difference
565 spectrum (that of *RaCCR1* from Fig. 1B in the main text is shown for comparison). (C) Peak
566 amplitude of *RaCCR1* photocurrents in response to 0.1 Hz trains of 6-ns laser flashes.

567 **Figure S7.** (A) A series of *RaCCR1* current traces in response to 1-s light pulses of different
568 intensities. (B and C) The dependence of peak current amplitude and desensitization on the
569 stimulus intensity in *RaCCR1* (B) and *RsCCR1* (C).

570 **Figure S8.** (A) A series of flash-induced absorption changes recorded at the indicated
571 wavelengths between 390 and 570 nm in purified *RsCCR1*. (B) Absorption changes at the
572 wavelengths corresponding to the K and L intermediates in the microsecond range in *RsCCR1*.

573 **Figure S9.** (A) Mean photoinduced absorbance changes recorded from purified *RaCCR1* in the
574 0-100 μ s time window. (B-F) Spectral transitions in *RaCCR1* derived by global fit analysis.

575 **Figure S10.** A laser-flash-evoked photocurrent trace recorded from *RaCCR1* (the black dashed
576 line) at the holding potential near the equilibrium potential for Na^+ . The red solid line shows a
577 multiexponential fit.

Rapidly desensitizing cation channelrhodopsins

1 **Table 1.** A list of BCCR homologs tested in this study (functional homologs are in bold font).

	Accession number	Abbreviated protein name	Source organism	Transcript number	Spectral peak (nm)
1	MN585290	<i>BfCCR1</i>	<i>Baffinella</i>	0987_20121128_7073*	500
2	MN585291	<i>BfCCR2</i>	<i>frigidus</i> (CCMP 2293)	0987_20121128_39196*	N/A
3	MN585292	<i>GcCCR1</i>	<i>Geminigera</i>	0799_20121207_13742*	N/A
4	MN585293	<i>GcCCR2</i>	<i>cryophila</i> (CCMP 2564)	0799_20121207_42824*	460
5	MN585294	<i>GICCR</i>	<i>Geminigera</i> sp. (Caron Lab isolate)	1102_20130122_14880*	N/A
6	MN585295	<i>HpCCR</i>	<i>Hanusia phi</i> (CCMP 325)	1048_20121227_6498*	500
7	MN585296	<i>HrCCR</i>	<i>Hemiselmis rufescens</i> (PCC 563)	1357_20121228_3699*	N/A
8	MN585298	<i>PsuCCR2</i>	<i>Proteomonas</i>	IRZA_2004242[#]	480
9	MN585297	<i>PsuCCR3</i>	<i>sulcata</i> (CCMP 704)	IRZA_2061044 [#]	N/A
10	MN585299	<i>PsuCCR4</i>		IRZA_2001844 [#]	N/A
11	MN585300	<i>RaCCR1</i>	<i>Rhodomonas</i>	1101_20121128_4039*	530

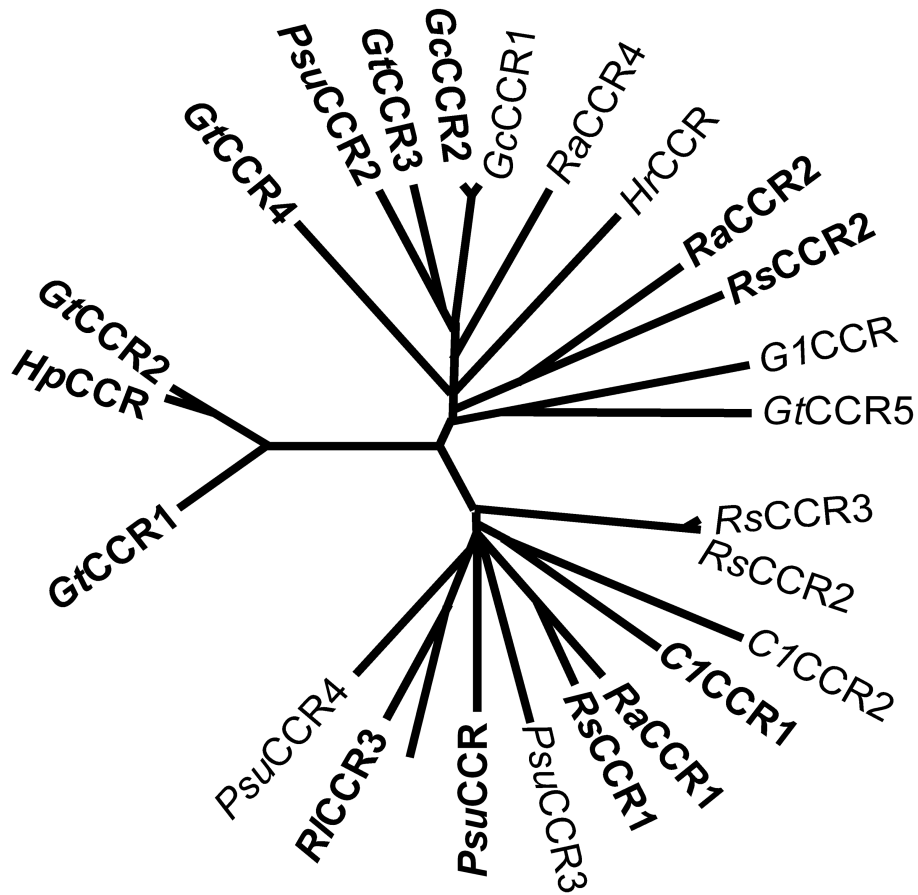
Rapidly desensitizing cation channelrhodopsins

12	MN585303	<i>RaCCR2</i>	<i>abbreviata</i>	1101_20121128_2696*	470
13	MN585301	<i>RaCCR3</i>	(Caron Lab	1101_20121128_32053*	520
14	MN585302	<i>RaCCR4</i>	isolate)	1101_20121128_22530*	N/A
15	MN585304	<i>RlCCR1</i>	<i>Rhodomonas</i>	0484_2_20121128_11058*	520
16	MN585305	<i>RlCCR2</i>	<i>lens</i> (CCMP 739)	0484_2_20121128_23336*	N/A
17	MN585307	<i>RsCCR1</i>	<i>Rhodomonas</i>	1047_20130122_18677*	524
18	MN585308	<i>RsCCR2</i>	<i>salina</i> (CCMP	1047_20130122_17846*	470
19	MN585306	<i>RsCCR3</i>	1319)	1047_20130122_11358*	N/A

2 *Transcripts from the MMETS project.

3 #Transcripts from the 1KP project.

A



B

1-s light pulse

